PHYSICAL REVIEW E **72**, 045201(R) (2005)

Spontaneous nucleation of localized peaks in a multistable nonlinear system

Umberto Bortolozzo,[1,2] René Rojas,[1] and Stefania Residori[1]
[1]*Institut Non-Linéaire de Nice, 1361 Route des Lucioles, 06560 Valbonne, France*
[2]*Istituto Nazionale di Ottica Applicata, Largo E. Fermi 6, 50125 Florence, Italy*
(Received 23 December 2004; published 7 October 2005)

In a nonlinear optical experiment we report a unique class of localized structures, which appears as localized peaks of a pattern nucleating over another pattern. We show that this occurs when the system is driven through three pattern branches of solutions, accompanied by the appearance of localized peaks with two different amplitudes. Spontaneous creation and motion of localized peaks are triggered by amplitude and phase fluctuations of the underlying pattern. The scenario is universal and applies whenever a subcritical bifurcation exists between two different pattern solutions.

DOI: 10.1103/PhysRevE.72.045201 PACS number(s): 05.45.−a, 42.65.Sf, 05.45.Yv, 47.54.+r

Localized structures are ubiquitous in nature [1], appearing in different fields of physics, chemistry, geophysics, etc. Several universal classes of localized states have been identified thus far [1,2]. However, an exhaustive classification of all possible types of localized states has not been available up to now. Starting from an experimentalist point of view, we can give a phenomenological classification of localized structures: those observed in thermal convection when there is bistability between a homogeneous state and a spatial pattern [3], localized pulses in Faraday instability [4], oscillons in vibrated grains [5], and cavity solitons in optics [6]. However, when looking to the phase space of solutions the situation is much more complex, and intriguing features of localized states may appear, such as their coupling in bound states [7], or their triangular shape, as recently observed in a liquid-crystal-light valve (LCLV) with optical feedback [8].

We report here a unique type of localized structures, which we call localized peaks, appearing as bright isolated spots over a spatial pattern of lower amplitude. We show that localized peaks exist whenever the system presents a subcritical bifurcation between two different pattern states. Creation and motion of localized peaks are spontaneously triggered by amplitude and phase fluctuations of the underlying pattern. These features of localized peaks, as well as the scenario for their appearance, are very general and can apply to any system showing coexistence between two different patterns. Note that temporally harmonic oscillons localized on a patterned background have been recently reported in parametrically driven surface waves in Newtonian fluids [9].

The experimental setup, consisting of a LCLV in an optical feedback loop, is the same as the one reported in [8]. The LCLV is composed of a nematic liquid-crystal film sandwiched in between a glass and a photoconductive plate over which a dielectric mirror is deposed. The liquid-crystal film is planar aligned (nematic director $\vec{n}$ parallel to the walls), with a thickness $d=15$ μm. Transparent electrodes over the glass plates permit the application of an external voltage V_0 across the liquid-crystal layer. The photoconductor behaves like a variable resistance, which decreases for increasing illumination. The feedback is obtained by sending back onto the photoconductor the light which has passed through the liquid-crystal layer and has been reflected by the dielectric mirror. The light beam experiences a phase shift which depends on the liquid-crystal reorientation and, in its turn, modulates the effective voltage that locally applies to the liquid crystals. The feedback loop is closed by an optical fiber bundle and is designed in such a way that diffraction and polarization interference are simultaneously present [8]. The optical-free propagation length is fixed to $L=-40$ mm. The angles of the polarizers are at 45° with respect to the liquid-crystal director $\vec{n}$. The free end of the fiber bundle is mounted on a precision rotation and translation stage in order to avoid rotation or translation in the feedback loop.

We fix a rms value of $V_0=12.3$ V, with a frequency 6 KHz. The period of the sinusoidal voltage V_0 is much shorter than the liquid-crystal response time and of the typical times for liquid-crystal hydrodynamics instabilities, such as electroconvection [10]. Thus, liquid crystals are sensitive only to the rms value of the applied voltage and perform a static reorientation. Hydrodynamical effects, such as backflow, are avoided and the molecular realignment is a pure Fréedericksz transition [11].

By increasing the input light intensity I_{in} we observe a sequence of transitions, as shown by the experimental snapshots of Fig. 1. The homogeneous steady-state loses stability and develops a pattern of hexagons that we call P_1 [Fig. 1(a)]. Pattern P_1 is due to diffraction in the optical feedback loop, which converts the phase modulation acquired by the light when passing through the LCLV into an intensity

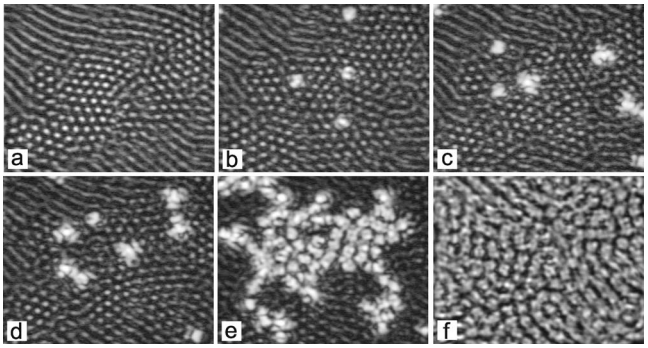

FIG. 1. Experimental snapshots showing the sequence of localized peaks appearance: I_{in}=(a) 0.32, (b) 0.38, (c) 0.40, (d) 0.41, (e) 0.42, and (f) 0.52 mW/cm^2.

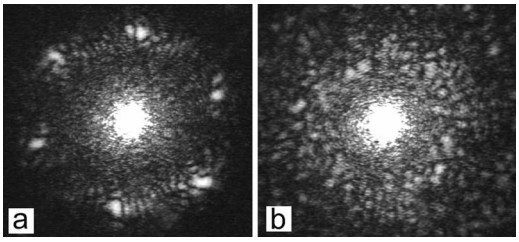

FIG. 2. Far-field images showing the change of critical wave number when passing from (a) P_1 to (b) P_3.

modulation. Due to the presence of the photoconductor, the intensity modulation changes, in its turn, the voltage applied to the liquid crystals and hence the phase shift on the incoming light beam. It is known that, under such a diffractive feedback, the LCLV system shows hexagonal patterns similar to P_1, with a spatial length that scales as $\sqrt{\lambda L}$, with λ being the optical wavelength and L the light free propagation length [12].

By further increasing I_{in}, localized peaks of higher amplitude appear over P_1 [Fig. 1(b)]. Then, localized peaks with a third higher value of the amplitude appear and coexist with the lower amplitude peaks, as shown in Figs. 1(c) and 1(d). We suppose the existence of a pattern $P_2(P_3)$, whose amplitude corresponds to that of the first (second) type of localized peaks, that we call, therefore, $P_{12}(P_{13})$. In a similar way, bistability between two different-amplitude localized structures has been attributed to the coexistence of two different patterns in the LCLV system [8]. By continuing to increase I_{in}, P_{13} peaks dominate over P_{12} and start to invade all space. By doing this, localized P_{13} peaks form large aggregations that propagate over the pinning sites of the underlying P_1 pattern. A typical picture of such a pinned aggregate is shown in Fig. 1(e), where a front can be distinguished between P_{13} and P_1. The front dynamics are characterized by the spontaneous nucleation of P_{13} peaks, as driven by the amplitude fluctuations of P_1. When I_{in} becomes sufficiently high for the pinned front to overcome the nucleation barrier, P_{13} peaks expand over all the available space, until pattern P_3 is formed [Fig. 1(f)].

The final state P_3 shows a dynamical behavior largely dominated by spatiotemporal chaos, with large local amplitude fluctuations and phase-driven motion of spatially uncorrelated domains. However, P_1 and P_3 are identified by the different values of their amplitude and also by their different spatial wavelengths and corresponding wave numbers. In Figs. 2(a) and 2(b) are displayed the far-field images corresponding to the spatial power spectra of P_1 and P_3, respectively, showing the change of critical wave number when passing from P_1 to P_3. The corresponding spatial wavelengths, measured in the near-field images, are $d_1=2\pi/q_1 \simeq 210\pm 30$ μm and $d_3=2\pi/q_3\simeq 290\pm 60$ μm for P_1 and P_3, respectively. Note that the q_3 spectral component is rather broadened by the space-time chaotic dynamics of P_3, whereas the spatial spectrum of P_1 is that of a hexagonal pattern. Concerning P_2, it is not possible to distinguish experimentally a pattern with an amplitude intermediate between P_1 and P_3. Indeed, P_2 always coexists with P_1 and P_3 and thus only manifests itself by the appearance of P_{12} peaks

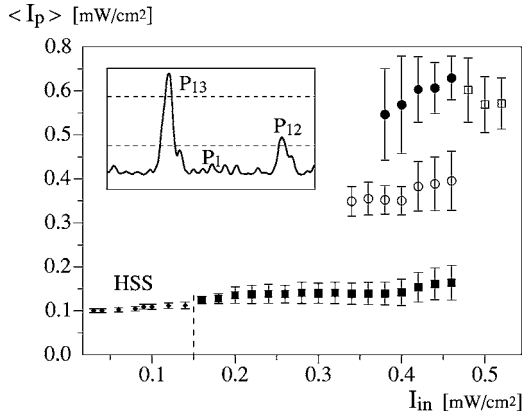

FIG. 3. Experimental bifurcation diagram $\langle I_p\rangle$ as a function of I_{in}. HSS: homogeneous steady state; filled squares (■): P_1; empty circles (○): P_{12}; filled circles (●): P_{13}; empty squares (□): P_3. In the inset is plotted a one-dimensional spatial intensity profile; the dashed lines are the thresholds applied to single out the three amplitude states.

nucleating spontaneously over P_1. For this reason, d_2 can only be evaluated as the width of individual P_{12} peaks and, thus, it is not strictly speaking a "wavelength." If we take the half-height width of P_{12} as an estimation of d_2, we find approximately the same value as for d_3.

We show in Fig. 3 the experimental bifurcation diagram: the pattern peak intensity $\langle I_p\rangle$ is plotted as a function of the input intensity I_{in}. The successive branches correspond, respectively, to the homogeneous steady state (HSS), losing stability with respect to P_1, and to P_{12} and P_{13} peaks, this last one becoming P_3 for high I_{in}. For each value of I_{in}, $\langle I_p\rangle$ is measured as an average of the pattern maxima by adopting the following procedure. By means of a computer interfaced charge-coupled device (CCD) camera, we record several near-field images. Then, we apply a threshold, in order to keep only the maxima of the patterns, and we make an ensemble average over the maxima. As schematically depicted in the inset of Fig. 3, when P_{12} and P_{13} coexist over the pattern P_1 we apply a double threshold filtering in such a way to single out the amplitude of P_1, P_{12}, and P_{13} into three separate frames. Then the three values of $\langle I_p\rangle$ are measured by making the ensemble average of all the maxima over each frame. The amplitudes of the three states being well separated, the resulting $\langle I_p\rangle$ values do not depend on the choice of the threshold level, as long as this level is changed approximately 10%, as we have verified. When decreasing I_{in}, we observe, both for P_{12} and P_{13}, the same bifurcation diagram as the one for increasing I_{in}. Hysteresis is prevented by the noise-induced mechanism of localized peaks creation, as these events are mainly driven by the amplitude fluctuations of P_1.

The theoretical model for our LCLV system was previously derived in [13] and consists of two coupled equations, one for the average director tilt $\theta(\vec{r},t)$, $0\leqslant\theta\leqslant\pi/2$, and one for the feedback light intensity I_w. The equation for the director reads as

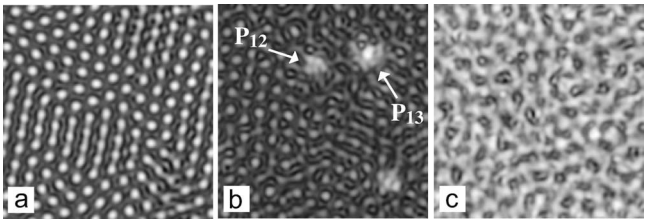

FIG. 4. Numerical snapshots of the angle θ corresponding to (a) P_1 (αI_{in}=1 V, θ_{max}=0.92 rad); (b) P_{12} and P_{13} (αI_{in}=2.6 V, θ_{max}=0.99 and 1.01 rad for P_{12} and P_{13}, respectively); (c) P_3 (αI_{in}=3 V, θ_{max}=1.02 rad).

$$\tau \partial_t \theta = l^2 \nabla_\perp^2 \theta - \theta + f(\theta), \tag{1}$$

where l is the electric coherence length, τ the local relaxation time, and $f(\theta)$ a function taking into account the response of the photoconductor to the feedback intensity I_w: $f(\theta)=0$ when $V \leqslant \Gamma V_{FT}$ and $f(\theta)=\pi/2(1-\sqrt{\Gamma V_{FT}/V})$ when $V>\Gamma V_{FT}$, with V the voltage that effectively applies to the liquid crystals

$$V = \Gamma V_0 + \alpha I_w(\theta), \tag{2}$$

and V_{FT} the threshold voltage for the Fréedericksz transition. Γ is the impedance of the LCLV dielectric layers and α a phenomenological parameter summarizing, in the linear approximation, the response of the photoconductor. After a free propagation length L, the feedback light intensity is given by

$$I_w = \frac{I_{in}}{4} \left| e^{i(L\lambda/4\pi)\nabla_\perp^2} (1 - e^{-i\beta \cos^2 \theta}) \right|^2, \tag{3}$$

the diffraction being accounted for by the operator $e^{i(L\lambda/4\pi)\nabla_\perp^2}$. Similar relationships between the tilt angle and the optical intensity distribution have been previously derived for light diffraction in electroconvective liquid-crystal cells, where far-field diffraction [14] or shadowgraph methods [15] were employed for pattern visualization, but without any feedback of light onto the tilt angle. Recently, electrohydrodynamic convection in a nematic liquid-crystal cell with a photoconductive electrode has been reported [16]. In such a case, though there was no feedback, the light beam was acting as an external photocontrol, locally modifying the voltage applied to the liquid crystal.

Anyway, the relationship between the tilt angle and the light intensity is very complicated, and a comparison between the light intensity pattern and the θ distribution inside the liquid-crystal cell is not straightforward. We have performed numerical simulations of our model, Eqs. (1)–(3), and we have found that, for the same values of I_{in}, near-field intensity patterns and θ patterns look very similar. The other parameters are Γ=0.3, α=5.5 V cm^2/mW, V_{FT}=3.5 V, l=30 μm, λ=632 nm, L=−40 mm. In Fig. 4 are displayed the numerical snapshots of θ corresponding to P_1, to P_{12}, P_{13}, and to P_3. By comparing with Fig. 1, we can see that θ patterns are in fairly good agreement with the experimental snapshots for the light intensity. Numerical simulations of a spin-1/2 atomic system with optical feedback, showing similar patterns, have been recently reported [17].

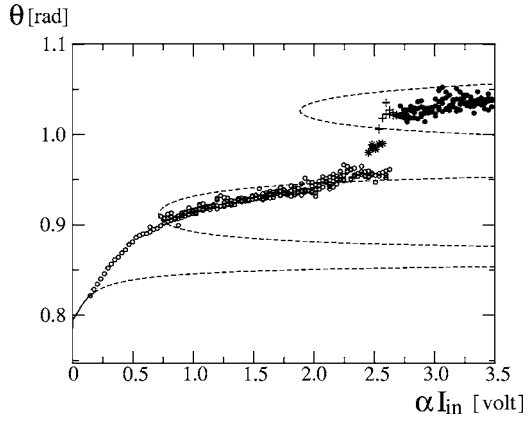

FIG. 5. Numerical bifurcation diagram for the maximum amplitude of θ as a function of αI_{in}: continuous (dashed) lines are the stable (unstable) HSS solutions θ_0; empty circles (○): hexagons P_1; stars (∗): localized peaks P_{12}; plus (+): localized peaks P_{13}; filled circles (●): space-time chaotic state P_3.

We study the linear stability of the spatial homogeneous solution θ_0 by writing $\theta=\theta_0+\varepsilon\theta_1 e^{\sigma t} e^{i\vec{q}\cdot\vec{r}}$, where θ_1 is the spatial perturbation and we find the dispersion relation $\sigma(q)$ for the most unstable modes: $\sigma=-q^2-1-\chi\cos(\Lambda q^2+\varphi_0/2)$, where $4\chi=\pi\alpha I_{in}\sqrt{\Gamma V_{FT}}\beta \sin(\varphi_0/2)\sin(2\theta_0)/[\Gamma V_0+\alpha I_{in}\sin^2(\varphi_0/2)]^{3/2}$, with $\Lambda=-\lambda L/4\pi l^2$ and $\varphi_0=\beta\cos^2\theta_0$. We show in Fig. 5 the HSS solutions θ_0 as a function of αI_{in}. These HSS are the same as the ones reported in [8,13] but in the present case the homogeneous state becomes unstable before the bistability with the upper homogeneous branch. The unstable point, which corresponds to the bifurcation to hexagons, can be controlled by changing the value of V_0. For each value of I_{in}, the most unstable modes for each HSS branch have a wave number q_1, q_2, and q_3, with $d_1=2\pi/q_1=190$ μm and $d_3=2\pi/q_3=260$ μm, consistent with the P_1 and P_3 pattern scales experimentally observed. In the same figure, Fig. 5, the numerical bifurcation diagram for the maximum amplitude of θ is plotted as a function of αI_{in}: empty circles are the hexagonal solution P_1; stars (plus) are localized peaks $P_{12}(P_{13})$; filled circles correspond to the space-time chaotic state P_3. Note that when the bifurcated P_1 branch meets the second HSS branch, the hexagonal pattern becomes irregular, showing amplitude fluctuations and defects. A similar phenomenon has been reported in a model describing the transition from hexagons to optical turbulence [18].

Note that in previous LCLV experiments, HSS was stable, thus localized structures were observed as single isolated spots over a spatially uniform background [8,13]. In the present experiments, HSS is unstable and leads to pattern P_1. Localized states are then nucleated spontaneously over a background which is spatially modulated. While in the case of an uniform background localized structures are created by local perturbations, either externally imposed or induced by inhomogeneities in the LCLV, in the case of a spatially modulated background localized peaks appear spontaneously due to the intrinsic dynamics of the system. Indeed, the creation of localized peaks is mainly due to the amplitude fluctuations of P_1, these fluctuations acting as a noise source that

continuously supplies to the system enough "energy" to jump from the lowest branch of solution to an upper one, with this one being that of P_2 or that of P_3 depending on the amplitude of the local fluctuation. Thus, both P_{12} and P_{13} peaks appear spontaneously, and continuously move during the time, as they are driven by the weakly chaotic dynamics of the underlying P_1 pattern. During their motion localized peaks follow the phase dynamics of P_1, slowly gliding and whirling around defect cores and domain walls [19].

In conclusion, we have identified a unique class of localized structures that we call localized peaks, appearing whenever two patterns coexist in the same region of parameters. We have shown the existence of such structures in a LCLV with optical feedback and have found their location through three pattern branches of solutions. We have also shown that localized peaks are spontaneously created by the amplitude fluctuations of the underlying pattern, which acts as a noise source triggering the onset of localized states. Phase fluctuations induce a weakly chaotic dynamics that drives the motion of localized peaks, diffusing randomly over the pinning sites of the underlying pattern. This scenario is quite a general one and should apply whenever a subcritical bifurcation exists between two different patterns.

We gratefully acknowledge P. L. Ramazza for having brought to our attention the existence of peak states in the LCLV and for helpful discussions. R.R. acknowledges financial support from Beca Presidente de la República of the Chilean Government. U.B. acknowledges financial support from the FUNFACS European Project, No. 2005-004/004868.

[1] M. Cross and P. Hohenberg, Rev. Mod. Phys. **65**, 851 (1993).
[2] S. Fauve and O. Thual, Phys. Rev. Lett. **64**, 282 (1990).
[3] J. Wu, R. Keolian, and I. Rudnick, Phys. Rev. Lett. **52**, 1421 (1984).
[4] W. S. Edwards and S. Fauve, J. Fluid Mech. **278**, 123 (1994).
[5] P. B. Umbanhowar, F. Melo, and H. L. Swinney, Nature (London) **382**, 793 (1996).
[6] M. Tlidi, P. Mandel, and R. Lefever, Phys. Rev. Lett. **73**, 640 (1994).
[7] B. Schäpers, M. Feldmann, T. Ackemann, and W. Lange, Phys. Rev. Lett. **85**, 748 (2000).
[8] U. Bortolozzo, L. Pastur, P. L. Ramazza, M. Tlidi, and G. Kozyreff, Phys. Rev. Lett. **93**, 253901 (2004).
[9] H. Arbell and J. Fineberg, Phys. Rev. Lett. **85**, 756 (2000).
[10] See, e.g., L. Kramer and W. Pesch, in *Pattern Formation in Liquid Crystals*, edited by A. Buka and L. Kramer (Springer-Verlag, New York, 1996).
[11] P. G. de Gennes and J. Prost, *The Physics of Liquid Crystals*, 2nd ed. (Oxford Science Publications, Clarendon, 1993).
[12] E. Pampaloni, S. Residori, and F. T. Arecchi, Europhys. Lett. **24**, 647 (1993).
[13] M. G. Clerc, A. Petrossian, and S. Residori, Phys. Rev. E **71**, 015205(R) (2005).
[14] T. O. Carroll, J. Appl. Phys. **43**, 767 (1972).
[15] S. Rasenat, G. Hartung, B. L. Winkler, and I. Rehberg, Exp. Fluids **7**, 412 (1989).
[16] M. Henriot, J. Burguete, and R. Ribotta, Phys. Rev. Lett. **91**, 104501-1 (2003).
[17] Yu. A. Logvin, B. Schäpers, and T. Ackemann, Phys. Rev. E **61**, 4622 (2000).
[18] D. Gomila and P. Colet, Phys. Rev. A **68**, 011801(R) (2003).
[19] Y-Nan Young, H. Riecke, and W. Pesch, New J. Phys. **5**, 135 (2003).